



Cite this: *Phys. Chem. Chem. Phys.*,
2023, 25, 19660

Effects of vacancies on the thermal conductivity of Si nanowires

Marc Túnica, ^{ab} Paolo Sebastiano Floris, ^a Pol Torres ^{ac} and
Riccardo Rurali ^{*a}

Point defects can be used to tailor the properties of semiconductors, but can also have undesired effects on electronic and thermal transport, particularly in ultrascaled nanostructures, such as nanowires. Here we use all-atom molecular dynamics to study the effect that different concentrations and spatial distributions of vacancies have on the thermal conductivity of Si nanowires, overcoming the limitations of previous studies. Although vacancies are not as effective as the nanovoids found in *e.g.* porous Si, they can still reduce the thermal conductivity in ultrathin Si nanowires by more than a factor of two, when found in concentrations smaller than 1%. We also present arguments against the so-called self-purification mechanism, which is sometimes suggested to take place and proposes that vacancies have no influence on transport phenomena in nanowires.

Received 20th April 2023,
Accepted 28th June 2023

DOI: 10.1039/d3cp01822a

rsc.li/pccp

1 Introduction

Semiconductors are privileged materials for electronic applications, because their resistivities can be varied by design with great control. The most efficient way to tune the carrier density is incorporating substitutional impurities, *i.e.* dopants, in the lattice.¹ Dopants are added on purpose to provide free carriers, but at the same time, especially in reduced dimensionality systems such as nanowires (NWs),^{2,3} they act as scattering centers,^{4–8} decreasing the mobility and limiting the performance of devices. Intrinsic defects, such as vacancies and self-interstitials, are lattice defects that do not need external impurities to be involved.^{9,10} Contrary to dopants, their presence is usually detrimental to the performances of electron devices (though important exceptions exist, see *e.g.* ref. 11 and 12): they can introduce deep levels in the bandgap that act as traps and they scatter carriers. The presence of vacancies, in particular, is often unavoidable. Vacancies can form as the result of an imperfect synthesis or when the annealing stage that follows ion implantation, if this technique is used to dope the material, cannot fully recover the perfect lattice structure. While there is extensive literature on the formation and effect of vacancies in bulk materials,⁹ they have been seldom studied in nanoscale systems. The general argument is that vacancies, similarly to

other point defects,^{4,13–17} prefer to sit next to the surface, where the lattice strain is more easily released. However, at variance with extrinsic impurities, when vacancies reach the surface they “annihilate”. This would lead to a “self-purification” effect that makes the presence of vacancies negligible or, at most, of little importance.

This simplified picture, however, has been questioned by the experimental results of Murphy *et al.*,¹⁸ who introduced vacancies in Si NWs by Ga⁺ ion-irradiation. The vacancies created were stable and their effect on phonon transport could be measured. In particular, they demonstrated that the effect of tensile strain on the thermal conductivity was greatly amplified by the presence of these lattice defects. Absence of self-purification was also reported in a theoretical study of Ge nanocrystals, where vacancies were predicted to be stable and to have a bulk-like behavior, without interacting strongly with the surface.¹⁹

Despite the interest that thermal transport in Si NWs has attracted,^{20–22} the role of vacancies has been overlooked. The effect of vacancies on the thermal conductivity of bulk Si was previously studied theoretically by different groups.^{23,24} The results are similar and feature a non-linear reduction of the thermal conductivity for an increasing concentration of vacancies. Interestingly, Wang *et al.*²³ considered both vacancies and nanovoids – like those of porous Si samples^{25,26} – and found that the latter are much more effective in reducing the thermal conductivity. The effect of vacancies on the thermal conductivity of Si NWs was studied by Gholipour Shahraki and Zeinali using reverse nonequilibrium molecular dynamics,²⁷ but their computational cell only allowed for a separation of 11 nm between the hot and the cold reservoir, and thus their results are likely to be severely

^a Institut de Ciència de Materials de Barcelona (ICMAB-CSIC), Campus de Bellaterra, 08193 Bellaterra, Barcelona, Spain. E-mail: rrurali@icmab.es

^b Laboratoire de Physique des Solides, Université Paris-Saclay, CNRS, Orsay 91405, France

^c Eurecat, Centre Tecnològic de Catalunya, Unit of Applied Artificial Intelligence, Av. Universitat Autònoma, 23, 08290 Cerdanyola del Vallès, Spain



affected by boundary scattering. Additionally, they obtained quite different results using the Tersoff²⁸ and the Stillinger–Weber²⁹ interatomic potential, finding a non-linear and a linear dependence of the thermal conductivity on the vacancy concentration, respectively. As none of these potentials was specifically parameterized to account for the vibrational or heat transport properties of Si, it is difficult to tell which of these results is more reliable (though the linear dependence seems to contradict the results obtained with analogous calculations in bulk Si^{23,24}). Similar calculations were carried out by Meem *et al.*³⁰ The separation between thermostats is in this case even shorter, amounting to only ~ 7 nm. Furthermore, they considered a very unusual and unrealistic distribution of vacancies, obtained by removing Si atoms along a line parallel to the wire axis.

In this paper we try to overcome the limitations of these studies by using the phonon optimized potential (POP) of Rohskopf and coworkers,³¹ which was specifically reparameterized to carefully reproduce the vibrational properties of Si. Importantly, this potential was also fitted against higher-order interatomic force constants (IFCs), those that determine phonon lifetimes, and thermal conductivity is in very good agreement with density-functional theory (DFT) results.³¹ Also, we use computational cells of at least ~ 90 nm and study the convergence of the thermal conductivity with the cell size, spanning lengths as large as 180 nm. As a preliminary step, we perform DFT calculations to study the dependence of the vacancy formation energy as a function of the radial coordinate, in order to assess the feasibility of surface segregation that could lead to the self-purification mechanism discussed above.

2 Computational methods

For the density-functional theory (DFT) calculations we use the Siesta code,^{32,33} an optimized double- ζ polarized basis set³⁴ and norm-conserving pseudopotentials.³⁵ Monovacancies are studied in $1 \times 1 \times 3$ supercells of a NW unit cell, sampling the Brillouin zone with the Γ point only, given the large size of the lattice vector along the periodic direction, *i.e.* ~ 3 nm. We carried out structural relaxations with the conjugate gradient method until all the forces were lower than 0.01 eV \AA^{-1} . The molecular dynamics (MD) calculations are performed with the LAMMPS package.³⁶ Interatomic forces are accounted for by means of the Phonon Optimized Potential (POP) of Rohskopf and coworkers,³¹ who reparameterized a bond-order potential of the Tersoff type²⁸ in order to improve the description of the vibrational properties. This interatomic potential yields both phonon dispersion and thermal conductivities that are in excellent agreement with those obtained with DFT.³¹ Si NWs are cut from the bulk, taking the axis to be along the $\langle 111 \rangle$ crystal direction. We considered diameters of 2.5 nm and 5 nm for the Siesta and LAMMPS calculations. In the case of DFT, the surface dangling bonds are passivated with H atoms to prevent reconstructions and electronic surface states.³⁷

The thermal conductivity is computed by means of approach-to-equilibrium molecular dynamics (AEMD). This method

consists in designing given initial nonequilibrium temperature conditions and then studying how the system reaches equilibrium once all constraints are released. In this work, we first carry out a thermalization step where we define two regions of equal size, which are equilibrated at two different temperatures, T_1 and T_2 . During the next step the two regions are allowed to gradually return to the equilibrium temperature, $(T_1 + T_2)/2$. At this point, it is possible to calculate the lattice thermal diffusivity by fitting the temperature difference $\Delta T(t) = \langle T_1 \rangle - \langle T_2 \rangle$ (where $\Delta T(t)$ denotes the time dependence of this quantity and the brackets denote an ensemble average) with a series of exponential functions that represent the solution to the Fourier equation of heat transport.

In this work we have set $T_1 = 400$ K and $T_2 = 200$ K; once a step-like temperature profile is established, we start the approach to the equilibrium step in the *NVE* ensemble. The thermal equilibrium corresponds to the temperature $T_{\text{eq}} = 300$ K (assuming that the system is spatially uniform with respect to the direction of heat transfer, which is the case in this work) and thus the thermal conductivity that we calculate is $\kappa(T_{\text{eq}})$. We consider the z -axis as the direction of heat transfer, and therefore the temperature difference between the two regions can be expressed as

$$\Delta T(t) = \sum_{n=1}^{\infty} C_n e^{-\alpha_n^2 \bar{\kappa}_z t} \quad (1)$$

where $\alpha_n = \frac{2\pi n}{L_z}$, L_z is the length of the nanowire, $\bar{\kappa}_z$ is thermal diffusivity and

$$C_n = 8(T_1 - T_2) \frac{[\cos(\alpha_n L_z/2) - 1]^2}{\alpha_n^2 L_z^2} \quad (2)$$

The lattice thermal conductivity is then obtained from

$$\kappa_z = \frac{\bar{\kappa}_z C_v}{V} \quad (3)$$

where $C_v = 3Nk_B$ is the heat capacity, obtained from the Dulong–Petit law, N being the number of atoms present in the system. As we are below the Debye temperature of Si, $T_D = 645$ K, we apply quantum corrections by renormalizing C_v by a factor \bar{q} , defined as the ratio between the simulation temperature and T_D . The limit for the summation in eqn (1) is set to $n = 20$, which is more than sufficient to get converged thermal conductivities.³⁸

3 Results and discussion

In order to assess the tendency to segregate towards the surface, we have mapped the formation energy³⁹ of monovacancies as a function of their radial coordinate. The nearsightedness of classical interatomic potentials, like the one here used for our MD computational experiments, could in principle lead to an underestimation of surface segregation. Therefore, to avoid these possible shortcomings, we have carried out these calculations within a fully quantum mechanical framework, using DFT. We followed two inequivalent paths going from the center of the NW



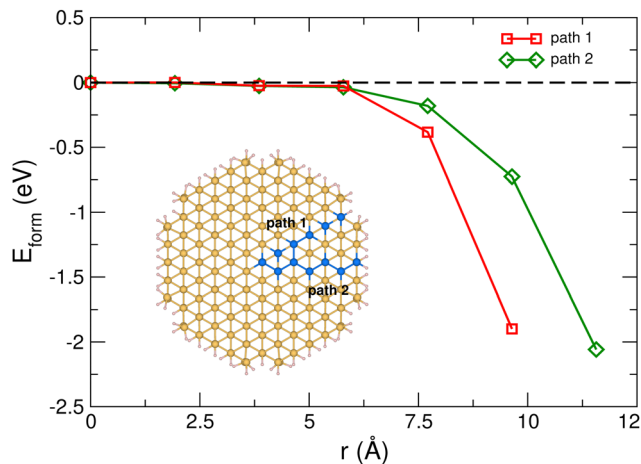


Fig. 1 Formation energy of Si vacancies as a function of their radial coordinate. Vacancies were created removing atoms along two different paths from the center to the surface of the NW, represented as dark blue spheres in the ball-and-stick cross-section view displayed in the inset.

to the surface. As can be seen in Fig. 1, we find that the formation energy is essentially unchanged with respect to the reference value, when the vacancy is at the center of the NW, for $r < 7 \text{ \AA}$. Then it moderately decreases ($r \sim 7.5 \text{ \AA}$) and only when it reaches a surface or subsurface location, we obtained a more pronounced variation. These values suggest that a vacancy in the innermost part of the NW is rather stable and does not seem likely to diffuse toward the surface. Additionally, to jump between the neighboring lattice sites, whose formation energies are tracked in Fig. 1, vacancies must also overcome a diffusion barrier that is expected to be sizeable. A quantitative characterization of the diffusivity of vacancies in Si NWs would require computing the potential energy surface (PES) and then using techniques such as the nudged elastic band (NEB) method to estimate the diffusion barrier, goals that are beyond the scope of this work. Nevertheless, our results qualitatively corroborate the experimental observations of Murphy *et al.*,¹⁸ who observed that vacancies in Si NWs are stable and have a measurable effect on the transport properties. It should also be noted that, due to the comparatively larger computational cost of DFT calculations, this study was performed in an ultrathin NW of only 2.5 nm of diameter. Although Si NWs of similar thickness have been reported experimentally,^{40–42} larger diameters of the order of several tens of nm are much more common. Therefore, the segregation effects that we obtain have to be considered an overestimation of the expected behavior in thicker Si NWs, because of their lower surface-to-bulk ratio.

After assessing the relative stability of vacancies at different radial coordinates, we carried out a series of MD computational experiments to study to what extent they can alter the thermal conductivity in Si NWs. We first study a radially uniform distribution of vacancies. Due to the inherently random nature of defect formation, for each target concentration we generate four independent distributions and averaged the corresponding thermal conductivities. Notice that, for each of these samples with the same nominal concentration, the actual number of vacancies in general differ a little from one sample

to the other, because of the probabilistic rule assumed to create the defects. As these variations are smaller, we plotted the data as a function of the average concentration.

The thermal conductivity obtained derives from different contributions: phonon–phonon collisions, boundary scattering due to radial confinement and boundary scattering due to the finite length of the NW. While the first two are physical contributions that need to be accounted for, the last is normally considered as a computational artifact, because realistic NWs are much longer than the samples used in atomistic simulations. A common way to get rid of this last term is based on Matthiessen's rule, which assumes that the different scattering mechanisms act independently and that scattering rates are additive. It consists in repeating the calculation of the thermal conductivity in increasingly long simulation cells, plotting $\kappa^{-1}(L_z^{-1})$ and taking the limit for $L_z^{-1} \rightarrow 0$, *i.e.* $L_z \rightarrow \infty$. The results of these calculations are shown in Fig. 2(a), where we report the averaged thermal conductivities, $\kappa(L_z)$, for four different values of L_z and five different concentrations of vacancies, c , plus the pristine Si NW for comparison. At all length scales the larger values of c result in higher thermal resistivities (*i.e.*, κ^{-1}), an indication that vacancies act as scattering centers of propagating heat-carrying phonons. From the same set of simulations we can plot the thermal conductivity accumulation function, defined as the ratio $\kappa(L_z)/\kappa_\infty$, κ_∞ being the extrapolated value of the thermal conductivity for an infinitely long NW of the same diameter. The results, displayed in Fig. 2(b), show that as the vacancy concentration increases, the relative contribution of phonons with long mean free path (mpf) also decreases. The extrapolated values of κ_∞ as a function of c are shown in Fig. 2(c). In this concentration range the decrease of the thermal conductivity can be fitted with an

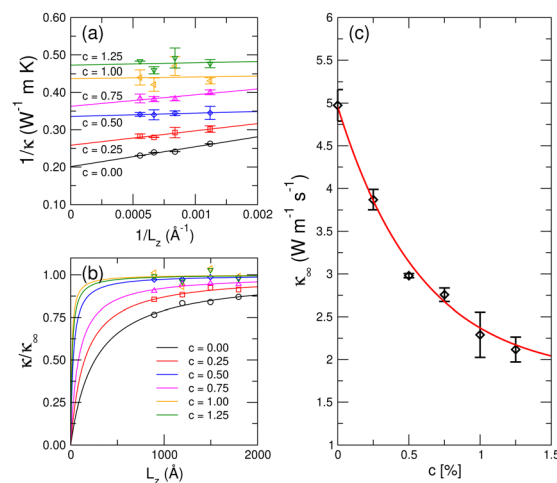


Fig. 2 (a) Inverse of κ as a function of the inverse of L_z for a NW with vacancy concentration $c = 0.00, 0.25, 0.50, 0.75, 1.00$, and 1.25% . The continuous lines are linear fits and the inverse of the y-axis intercept is taken as the converged value, κ_∞ , for that concentration, c . (b) Ratio of $\kappa(L_z)/\kappa_\infty$ for $c = 0.00, 0.25, 0.50, 0.75, 1.00$, and 1.25% . (c) Thermal conductivity, κ_∞ , as estimated by means of the linear fits of panel (a) as a function of the vacancy concentration, c . The continuous line is an exponential fit of the computed values.



exponential decay of the type $\kappa_{\infty}^{\text{prist}} e^{-c/x}$, where $\kappa_{\infty}^{\text{prist}}$ is the thermal conductivity of a pristine Si NW, extrapolated for $L \rightarrow \infty$. As it can be seen, modest concentrations of vacancies yield a considerable reduction of the thermal conductivity, e.g. for $c = 0.5\%$, κ is almost halved. Larger defect concentrations were not considered because of their little significance in experiments and also because the system becomes numerically more difficult to handle, with a non negligible probability for clusters of atoms to leave the surface of the NW, resulting in severe instabilities. Notice that our results are valid for small concentrations of vacancies. At larger concentrations, the aggregation of vacancies leading to the formation of divacancies or small cluster – which has been shown to be energetically favoured⁴³ – cannot be neglected. This limit, where nanovoids form, has been previously addressed in detail by studies focused on porous Si NWs.^{25,44}

When we have discussed the segregation energy diagram of Fig. 1 we concluded that a scenario where vacancies diffuse to the surface and then annihilate, leaving behind at most some kind of surface roughness, does not appear to be very likely on the basis of total energy considerations. Therefore, the absence of vacancies in Si NWs cannot be taken for granted. However, in the immediacy of the surface there exists a non-negligible segregation tendency (see the values of E_{form} for $r > 7.5$ Å in Fig. 1) and, although they must overcome some diffusion barriers, vacancies are indeed expected to move outward. If vacancies in the innermost part of the NW are not mobile and only those very close to the surface can segregate (and then annihilate), one can figure a situation where an outer ring, close to the surface, is fully depleted of vacancies, which are only present in the inside of the NW.

To address this scenario, we computed the thermal conductivity of different nonuniform distributions of vacancies. We considered a fixed number of vacancies, those that if uniformly distributed would result in a concentration of 0.5%, and constructed the following distributions: (a) all vacancies lie inside a cylinder of radius 5, 10, and 15 Å; (b) all vacancies lie within a ring of thickness 5, 10, 15, and 20 Å, centered at $r = 12.5$ Å; (c) vacancies follow a Gaussian distribution with maximum at the NW center and full width half maximum (FWHM) equal to 2.35, 25.90, and 40.03 Å. Additionally, despite its scarce experimental relevance, we also considered the case where all vacancies lie outside a cylinder of radius 5, 10, and 15 Å. The calculated thermal conductivity, plotted as a function of the cross-section of the defective region, S , is shown in Fig. 3. As it can be seen, the hard-wall confinement within a given radius or the Gaussian distribution behave qualitatively in the same way: as S increases, κ decreases because the concentration in the defective region decreases as well. Similar results are obtained with the rather artificial distribution where vacancies are confined within an annulus with average radius, $r = 12.5$ Å. On the other hand, when vacancies are forced to lie next to the surface, we obtain larger values of κ , indicating that vacancies are much more effective in scattering phonons when they are concentrated in the innermost part of the NW or, at least, sufficiently far from the surface, as suggested by the results of the annulus distribution that exhibit a qualitatively similar behavior. In the case of surface vacancies, we

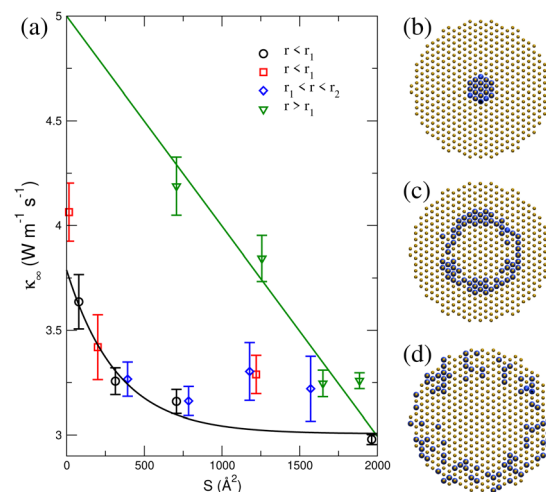


Fig. 3 (a) Thermal conductivity, κ_{∞} , as a function of the cross-section of the defective region, S (in the case of the Gaussian distribution we have taken as an effective confinement radius a value such that outside of it, no vacancies were found). The continuous lines are an exponential and a linear fit to the case $r < r_1$ and $r > r_1$ (see text). Cross-section view of a NW with a distribution of vacancies of the type (b) $r < r_1$, (c) $r_1 < r < r_2$, and (d) $r > r_1$; Si atoms and vacancies are represented by yellow and blue spheres, respectively.

found that the dependence of κ on S can also be predicted by computing the total thermal resistance as the parallel of the resistance of a pristine, R_{pure} , and a defective NW, R_{d} , i.e. $R_{\text{tot}}^{-1} = R_{\text{pure}}^{-1} + R_{\text{d}}^{-1}$. The thermal conductivity obtained in this way is displayed as a continuous green line in Fig. 3.

These results agree with previous reports based on nonequilibrium Green's functions (NEGF) where the scattering of individual vacancies was addressed.⁴⁵ Vacancies in the innermost part of the NW were found to be more effective in reducing the conductance, despite the lower degree of structural distortion associated, than vacancies next to the NW surface. Similar conclusions were reached by the one-dimensional distribution of vacancies considered in ref. 30.

Our preliminary DFT calculations indicated that surface segregation of vacancies in Si NWs does not seem likely and thus self-purification should not be a mechanism at play. Corroborating these conclusions in a dynamical calculation, and seeing if they hold at finite temperature as well, is not feasible, because diffusion typically takes place over timescales that are much longer than those that can be spanned with MD. Also, we found that diffusion barriers are overestimated, if compared to DFT, by the interatomic potential here employed. Yet, we have verified that vacancies do not migrate during one of our typical runs to calculate the thermal conductivity to ensure the robustness of our computed values. To this end we have monitored the position of the vacancies in the case of a uniform distribution in a NW 90 nm long, in a 1.5 ns NVT MD run at 300 K. This, for the reasons discussed above, has a significance that is more numerical (i.e., the samples are stable and the vacancy distribution does change significantly during the simulation) than physical. In Fig. 4 we track the position of the Si atoms with less than four neighbors, which indirectly



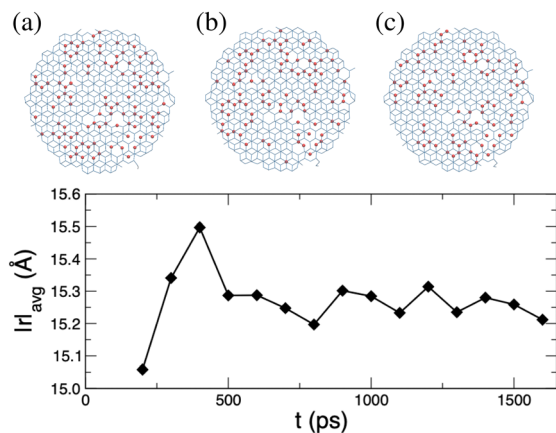


Fig. 4 Average distance from the NW center of a uniform distribution of vacancies during an NVE run as a function of time. The panels show snapshots at (a) $t = 200$ ps, (b) $t = 800$ ps, and (c) $t = 1.5$ ns of slabs 5 Å at the center of the NW. The red spheres represent atoms less than four-fold coordinated, which thus indicate the presence of a vacancy nearby.

indicate the presence of a nearby vacancy. As can be seen in Fig. 4, the average distance of the under-coordinated Si atoms from the NW center, $|r|$, remains essentially unaltered throughout the dynamics. Despite some fluctuations, particularly in the beginning where possibly the system was not yet well equilibrated, there is no trend indicating any kind of migration of the vacancies toward the surface. These results indicate that in our computational experiments, the vacancy distributions are rather stable and are not altered significantly, let alone surface segregation, which is not observed.

4 Conclusions

In summary, we have studied the effect of vacancies on the thermal conductivity of Si NWs. We have shown that moderate concentrations of vacancies, e.g. $c \sim 0.75\%$, are very effective in scattering phonons and thus reducing the thermal conductivity. When looking at nonuniform radial distributions, we found that vacancies that are mostly located in the innermost part of the NW are much more effective in reducing the thermal conductivity. These calculations are based on a newly developed bond-order potential that has been specifically developed to account for the vibrational properties of Si and that predicts its bulk thermal conductivity with an accuracy comparable to DFT calculations. Finally, we presented qualitative arguments that suggest that, in agreement with experimental results, vacancies in ultrathin NWs are not expected to diffuse to the surface. Consequently, the mechanism of self-purification, wherein vacancies reach the surface and annihilate, is unlikely to occur, at least under close-to-equilibrium conditions. These findings underscore the need to assess the impact of the presence of monovacancies on electronic and thermal transport in nanostructured Si.

Conflicts of interest

There are no conflicts to declare.

Acknowledgements

This work was financially supported by the European Commission through the Marie Skłodowska-Curie projects HORATES (GA-955837), by MCIN/AEI/10.13039/501100011033 under grant PID2020-119777GB-I00, and the Severo Ochoa Centres of Excellence Program under grant CEX2019-000917-S, and by the Generalitat de Catalunya under grant no. 2021 SGR 01519. Calculations were performed at the Centro de Supercomputación de Galicia (CESGA) within action FI-2022-1-0018 of the Red Española de Supercomputación (RES). We thank Antonio Cappai and Miguel Rubí for useful discussions.

References

- 1 R. S. Muller and T. I. Kamins, *Device Electronics for Integrated Circuits*, John Wiley & Sons, Hoboken, NJ, 1986.
- 2 W. Lu and C. M. Lieber, *J. Phys. D: Appl. Phys.*, 2006, **39**, R387–R406.
- 3 R. Rurali, *Rev. Mod. Phys.*, 2010, **82**, 427–449.
- 4 M. V. Fernández-Serra, C. Adessi and X. Blase, *Phys. Rev. Lett.*, 2006, **96**, 166805.
- 5 M.-V. Fernández-Serra, C. Adessi and X. Blase, *Nano Lett.*, 2006, **6**, 2674–2678.
- 6 T. Markussen, R. Rurali, M. Brandbyge and A.-P. Jauho, *Phys. Rev. B: Condens. Matter Mater. Phys.*, 2006, **74**, 245313.
- 7 T. Markussen, R. Rurali, A.-P. Jauho and M. Brandbyge, *Phys. Rev. Lett.*, 2007, **99**, 076803.
- 8 R. Rurali, T. Markussen, J. Suñe, M. Brandbyge and A.-P. Jauho, *Nano Lett.*, 2008, **8**, 2825–2828.
- 9 P. M. Fahey, P. B. Griffin and J. D. Plummer, *Rev. Mod. Phys.*, 1989, **61**, 289–384.
- 10 H. J. Queisser and E. E. Haller, *Science*, 1998, **281**, 945–950.
- 11 J. R. Weber, W. F. Koehl, J. B. Varley, A. Janotti, B. B. Buckley, C. G. V. de Walle and D. D. Awschalom, *Proc. Natl. Acad. Sci. U. S. A.*, 2010, **107**, 8513–8518.
- 12 M. Ai, J.-W. Zhang, Y.-W. Wu, L. Pan, C. Shi and J.-J. Zou, *Chem. – Asian J.*, 2020, **15**, 3599–3619.
- 13 H. Peelaers, B. Partoens and F. Peeters, *Nano Lett.*, 2006, **6**, 2781–2784.
- 14 N. Fukata, S. Ishida, S. Yokono, R. Takiguchi, J. Chen, T. Sekiguchi and K. Murakami, *Nano Lett.*, 2011, **11**, 651–656.
- 15 M. Amato, M. Palumbo and S. Ossicini, *Phys. Status Solidi B*, 2010, **247**, 2096.
- 16 M. Galicka, R. Buczko and P. Kacman, *J. Phys. Chem. C*, 2013, **117**, 20361–20370.
- 17 M. Amato, S. Ossicini, E. Canadell and R. Rurali, *Nano Lett.*, 2019, **19**, 866–876.
- 18 K. F. Murphy, B. Piccione, M. B. Zanjani, J. R. Lukes and D. S. Gianola, *Nano Lett.*, 2014, **14**, 3785–3792.
- 19 K. Bayus, O. Paz and S. P. Beckman, *Phys. Rev. B: Condens. Matter Mater. Phys.*, 2010, **82**, 155409.
- 20 S. G. Volz and G. Chen, *Appl. Phys. Lett.*, 1999, **75**, 2056–2058.



- 21 D. Li, Y. Wu, P. Kim, L. Shi, P. Yang and A. Majumdar, *Appl. Phys. Lett.*, 2003, **83**, 2934–2936.
- 22 M. Hu, K. P. Giapis, J. V. Goicochea, X. Zhang and D. Poulikakos, *Nano Lett.*, 2011, **11**, 618–623.
- 23 T. Wang, G. K. H. Madsen and A. Hartmaier, *Modell. Simul. Mater. Sci. Eng.*, 2014, **22**, 035011.
- 24 Y. Lee, S. Lee and G. S. Hwang, *Phys. Rev. B: Condens. Matter Mater. Phys.*, 2011, **83**, 125202.
- 25 X. Cartoixà, R. Dettori, C. Melis, L. Colombo and R. Rurali, *Appl. Phys. Lett.*, 2016, **109**, 013107.
- 26 S. A. Hosseini, A. Davies, I. Dickey, N. Neophytou, P. A. Greaney and L. de Sousa Oliveira, *Mater. Today Phys.*, 2022, **27**, 100719.
- 27 M. Gholipour Shahraki and Z. Zeinali, *J. Phys. Chem. Solids*, 2015, **85**, 233–238.
- 28 J. Tersoff, *Phys. Rev. B: Condens. Matter Mater. Phys.*, 1989, **39**, 5566–5568.
- 29 F. H. Stillinger and T. A. Weber, *Phys. Rev. B: Condens. Matter Mater. Phys.*, 1985, **31**, 5262–5271.
- 30 A. U. H. Meem, O. Chowdhury and A. M. Morshed, *Micro Nano Lett.*, 2018, **13**, 1146–1150.
- 31 A. Rohskopf, H. R. Seyf, K. Gordiz, T. Tadano and A. Henry, *npj Comput. Mater.*, 2017, **3**, 27.
- 32 J. M. Soler, E. Artacho, J. D. Gale, A. García, J. Junquera, P. Ordejón and D. Sánchez-Portal, *J. Phys.: Condens. Matter*, 2002, **14**, 2745–2779.
- 33 E. Artacho, E. Anglada, O. Diéguez, J. D. Gale, A. García, J. Junquera, R. M. Martín, P. Ordejón, J. M. Pruneda, D. Sánchez-Portal and J. M. Soler, *J. Phys.: Condens. Matter*, 2008, **20**, 064208.
- 34 E. Anglada, J. M. Soler, J. Junquera and E. Artacho, *Phys. Rev. B: Condens. Matter Mater. Phys.*, 2002, **66**, 205101.
- 35 N. Troullier and J. L. Martins, *Phys. Rev. B: Condens. Matter Mater. Phys.*, 1991, **43**, 1993–2006.
- 36 S. Plimpton, *J. Comput. Phys.*, 1995, **117**, 1–19.
- 37 R. Rurali, A. Poissier and N. Lorente, *Phys. Rev. B: Condens. Matter Mater. Phys.*, 2006, **74**, 165324.
- 38 C. Melis, R. Dettori, S. Vandermeulen and L. Colombo, *Eur. Phys. J. B*, 2014, **87**, 96.
- 39 R. Rurali and X. Cartoixà, *Nano Lett.*, 2009, **9**, 975–979.
- 40 A. M. Morales and C. M. Lieber, *Science*, 1998, **279**, 208–211.
- 41 D. D. D. Ma, C. S. Lee, F. C. K. Au, S. Y. Tong and S. T. Lee, *Science*, 2003, **299**, 1874–1877.
- 42 T. W. Nam and J. C. Grossman, *Nano Lett.*, 2023, **23**, 2347–2353.
- 43 A. Bongiorno and L. Colombo, *Phys. Rev. B: Condens. Matter Mater. Phys.*, 1998, **57**, 8767–8769.
- 44 P. Ferrando-Villalba, L. D'Ortenzi, G. G. Dalkiranis, E. Cara, A. F. Lopeandia, L. Abad, R. Rurali, X. Cartoixà, N. De Leo, Z. Saghi, M. Jacob, N. Gambacorti, L. Boarino and J. Rodríguez-Viejo, *Sci. Rep.*, 2018, **8**, 12796.
- 45 K. Yamamoto, H. Ishii, N. Kobayashi and K. Hirose, *Appl. Phys. Express*, 2011, **4**, 085001.

